Solvothermal synthesis, characterisation and luminescent property of multilayered SnO_2 hollow microspheres

Zhi Yuan Wang, Feng Ping Wang, Yan Li, Ming Yan Li, Muhammad Zubair Iqbal, Qurat-Ul-Ain Javed, Yan Zhen Lu, Mei Xu, Quan Shui Li

Department of Physics, School of Mathematics and Physics, University of Science and Technology Beijing, Beijing 100083, People's Republic of China
E-mail: fpwang@ustb.edu.cn

Published in Micro & Nano Letters; Received on 29th November 2013; Revised on 24th January 2014; Accepted on 28th January 2014

Multilayered nanocrystalline SnO_2 hollow microspheres (MHS-SnO_2) of a rutile structure with a controllable morphology have been successfully synthesised via a chemically induced self-assembly method by using tin chloride pentahydrate and sucrose as precursors in the glycol–water aided solvothermal synthesis. The morphology, composition, structure and luminescent properties of MHS-SnO_2 are characterised by field-emission scanning electron microscopy (FESEM), transmission electron microscopy (TEM), high-resolution transmission electron microscopy (HRTEM) with selected area electron diffraction, X-ray diffraction, Raman spectroscopy and photoluminescence spectroscopy. The FESEM, TEM and HRTEM images indicate that the as-prepared microspheres show a multilayer structure and the walls of the hollow microspheres are composed of single crystalline nanoparticles . The effect of calcinating temperature on the Raman and optical properties of the product is analysed and a self-assembly growth mechanism of the MHS-SnO_2 is proposed .

1. Introduction: As an *n*-type semiconductor with a direct optical bandgap ($E_g = 3.6$ eV) [1], SnO_2 is one of the most promising materials because of its many potential applications. Many chemical and physical methods have been used to prepare tin oxide micro and nanostructures such as thermal decomposition, thermal chemical vapour deposition (CVD), solvothermal, RF sputtering, the hydrothermal method, the sol–gel method and surfactant assisted methods [1, 2]. Among the chemical methods, the solvothermal approach has more advantages compared with above-mentioned methods in several aspects, such as simple manipulation, low reaction temperature, short processing time and less complicated equipment being involved [3].

In the past few years, great efforts have been devoted to fabricating SnO_2 hollow microspheres because of their large specific surface area and variety of applications, such as gas sensors [4], solar cells [5], photocatalysis [6], the delivery and controlled release of drugs [7] and anode materials [8]. Wang *et al.* [9] synthesised crystalline SnO_2 hollow spheres and studied their performance for reversible Li-ion storage. Lu [10] reported template-based and template-free hydrothermal approaches which are suitable for the mass production of tin oxide hollow spheres and can be used to coat SnO_2 onto other materials to form other hollow nanostructures. Tin oxide, as the next generation of anodic material for Li-ion batteries, has high theoretical capacity. The SnO_2 hollow microspheres can provide sufficient space to buffer the charging–discharging process and improve the properties of lithium batteries [8].

Yang *et al.* [1] have successfully synthesised multilayered nanocrystalline SnO_2 hollow microspheres under hydrothermal conditions using water as the solvent, sucrose and tin tetrachloride pentahydrate as reactants and showed good performance in electrochemical characteristics. However, the synthesis of nanocrystalline SnO_2 hollow microspheres with uniform size and favourable dispersity under facile conditions is still a big challenge.

In the present work, we have used the mixture of glycol–water (V_{water}:V_{glycol} = 1:1) as the solvent and changed the amount of reactants, successfully synthesising multilayered nanocrystalline SnO_2 hollow microspheres with a smooth surface, uniform size and good dispersity. The effect of calcinating temperature on the Raman and luminescent properties of the as-prepared product is discussed in detail and a self-assembly growth mechanism of the multilayered nanocrystalline SnO_2 hollow microspheres (MHS-SnO_2) is proposed .

2. Experimental details

2.1. Sample preparation: All the chemical reagents used in this work were of analytical grade and used without further purification. In a typical experimental procedure, 2.80 g of $SnCl_4{\cdot}5H_2O$ (8 mmol), 6.84 g of sucrose (20 mmol), 20 ml of distilled water and 20 ml of glycol (V_{water}:V_{glycol} = 1:1) were transferred to a beaker and stirred for 10 min to form a homogeneous solution. Subsequently, the solution was transferred into a 50 ml Teflon-lined stainless steel autoclave and kept at 180°C for 24 h. Then, the black SnO_2–C composite was collected and washed with distilled water and ethanol three times, and dried in an oven at 80°C. The prepared SnO_2–C composite was calcinated in a muffle furnace at 550, 750 and 950°C for 4 h.

2.2. Characterisation: The morphology of the as-prepared product was studied using a Hitachi S-3500 field emission scanning electron microscope (FESEM) and a Tecnai G^2 F30 S-TWIN transmission electron microscope (TEM). The crystal structure of the obtained sample was characterised by X'Pert MPD powder X-ray diffraction (XRD) with a copper target and K_α radiation (λ = 0.154056 nm). Raman spectra were recorded with 532 nm wavelength excitation at room temperature, using a Horiba Jobin Yvon LabRAM HR800. The room temperature photoluminescence (PL) emission spectra were investigated using the Hitachi F-4500 fluorescence spectrometer with a Xe lamp as the excitation source.

3. Results and discussion

3.1. Morphology and structure: All of the samples calcinated at different temperatures present the consistent morphology. Fig. 1 shows the typical SEM and TEM images of the as-prepared product calcinated at 550°C. As shown in Fig. 1*a*, the product prepared using water and glycol (V_{water}:V_{glycol} = 1:1) as the solvent exhibits-spherical and uniform shape with diameter in the range of 2–3 μm. The open hole in the surface of the as - prepared spheres (Fig. 1*b*) may be because of the gasification and removal of inner carbon. Through the open hole, the inside

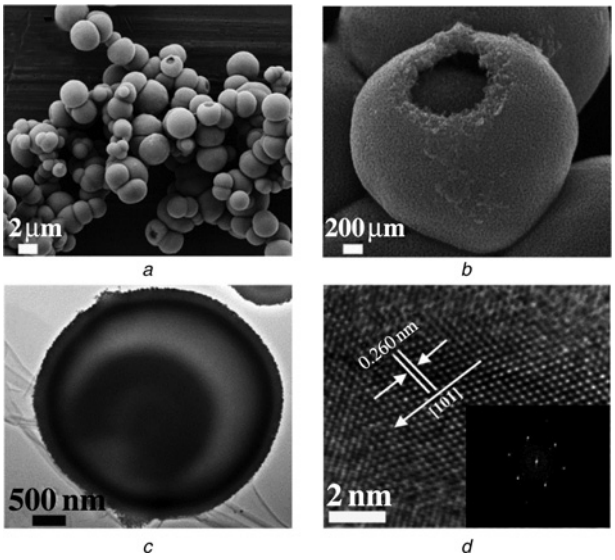

Figure 1 *Typical SEM, TEM, and HRTEM image of the as-synthesised product*
a, *b* SEM image
c TEM image
d HRTEM image

smaller sphere and hollow structure can be clearly seen, indicating the as-prepared SnO_2 microstructures have a multilayered hollow structure. Moreover, the outer shell of the SnO_2 microsphere is composed of aggregated nanoparticles, with the thickness of about 200 nm. Compared with the previous study of Yang *et al.* [1], the current synthetic MHS-SnO_2 is more uniform and has better dispersiveness with a smooth surface.

To obtain insight into the morphology of the MHS-SnO_2, transmission electron microscopy has been used to visualise the detailed structure of the as-prepared architectures. As shown in Fig. 1*c*, the micrograph clearly exhibits that the microspheres prepared by using water and glycol (V_{water}:V_{glycol} = 1:1) as solvent possess hollow structure, in which there is a smaller sphere. Through careful examination, a third layer can be observed from the contrast of light and shade, indicating the as-prepared product is three layered structure. The high-resolution TEM (HRTEM) lattice image of a MHS-SnO_2 is shown in Fig. 1*d*. The measured interplanar spacing in the fringe of the MHS-SnO_2 is 0.260 nm, which is consistent with the interplanar spacing value of 0.264 nm for the {101} lattice planes of rutile SnO_2. The corresponding selected area electron diffraction pattern as shown in the inset of Fig. 1*d* indicates that the prepared material is composed of single crystalline nanoparticles.

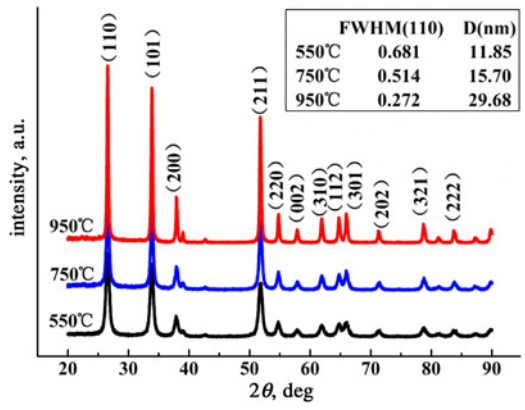

Figure 2 *X-ray diffraction patterns of MHS-SnO_2 calcinated at different temperatures*

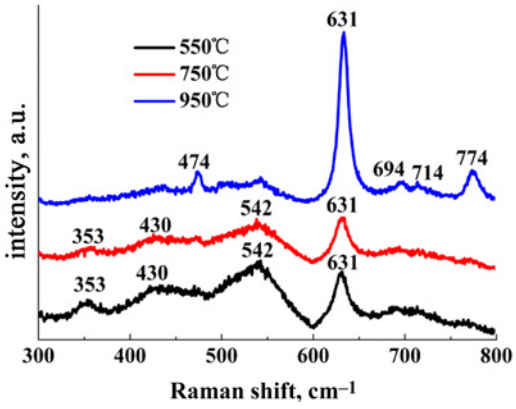

Figure 3 *Raman spectra of MHS-SnO_2 calcinated at different temperatures*

The XRD patterns of the products are shown in Fig. 2. All the diffraction peaks of the samples can be indexed to rutile SnO_2 (JCPDS Card No. 41-1445, p42/mnm, $a = b = 4.738$ Å, $c = 3.187$ Å and $\alpha = \beta = \gamma = 90°$). No other diffraction peaks for impurities are detected, indicating that the final synthesised products are of pure single phase. The strong and sharp diffraction peaks reveal that the as-prepared SnO_2 is well crystallised.

As shown from Fig. 3, the intensity of the XRD increases dramatically and the full-width at half-maxima (FWHM) decreases obviously, respectively, with increasing the annealing temperature, which indicates that the crystallinity of the samples is improved by high-temperature calcination. The crystallite size (D) can be calculated according to the Debye-Scherer formula

$$D = 0.89\lambda/\beta\cos\theta \tag{1}$$

where θ is the Bragg angle and β is the FWHM, λ is the X-ray wavelength (1.5406 Å) in the Cu K_α radiation. FWHM and crystalline size determined from (110) diffraction peak are listed in Fig. 2. The calculated crystallite size of MHS-SnO_2 calcinated at 550, 750 and 950°C is about 11.85, 15.70 and 29.68 nm, respectively.

3.2. Raman: The vibration properties of MHS-SnO_2 are investigated by Raman scattering techniques at room temperature. Rutile SnO_2 belongs to the space group D_{4h}^{14}, of which the normal lattice vibration at the Γ point of the Brillouin zone is given on the basis of group theory [11]

$$\Gamma = 1A_{1g} + 1A_{2g} + 1A_{2u} + 1B_{1g} + 1B_{2g} + 2B_{1u} + 1E_g + 3E_u \tag{2}$$

Within these modes, B_{1g}, E_g, A_{1g} and B_{2g} are the Raman active and A_{2u} and E_u are the IR active, while A_{2g} and B_{1u} are the inactive. E_g is the only mode which vibrates parallel to the C-axis in all of the Raman active modes while the other Raman active modes vibrate in the plane perpendicular to the C-axis [11]. In addition, it is hard to find the peak of B_{1g} (123 cm^{-1}) mode because of the existence of a strong Rayleigh scattering peak.

Fig. 3 shows the room-temperature Raman scattering spectra of MHS-SnO_2 calcinated at 550, 750 and 950°C. For the products calcinated at 550 and 750°C, a Raman-active mode A_{1g} located at 631 cm^{-1} and three non-Raman active peaks at 353, 430, 542 cm^{-1} are observed. The three non-Raman active peaks become weak with increasing calcinating temperature and almost disappear when the calcinating temperature reaches 950°C. Raman spectra are very sensitive to the crystalline size and the imperfections on the particle surface, such as oxygen vacancies and lattice disorder, are likely to relax the selection rules, which may result in the transformation from non-Raman active modes to Raman active modes [12–13].

doi: 10.1049/mnl.2013.0681

Therefore these three non-Raman active peaks can be attributed to defects such as lattice disorder and oxygen vacancies in the as-prepared nanostructures.

For the product calcinated at 950°C, five peaks occur at 474, 631, 694, 714 and 774 cm^{-1}. The peaks at 474, 631 and 774 cm^{-1} are attributed to fundamental Raman-active modes E_g, A_{1g} and B_{2g}, respectively, which is in good agreement with those for the rutile bulk SnO_2. The peak at 694 cm^{-1} can be assigned to IR-active A_{2u}, which can be attributed to the breakdown of the selection rules or imperfections on the particle surface [11, 12]. The weak peak at 714 cm^{-1} can be designated to IR-active mode E_u (LO) and has rarely been reported. We deduce that the IR-active mode E_u (LO) transforms into the Raman active mode when crystal symmetry is reduced. In addition, it can be also observed that the Raman-active peaks become stronger and sharper with increasing calcinating temperature.

3.3. Growth mechanism: Here, a growth mechanism for the as-prepared MHS-SnO_2 is proposed as illustrated schematically in Fig. 4 based on the above careful structural analysis and the growth mechanism of the multilayered hollow sphere [14]. In the glycol–water (V_{water}:V_{glycol} = 1:1) solvothermal synthesis, the primary small carbon particles are formed via dehydration of sucrose (step I) and these particles are hydrophilic owing to the existence of the OH group on the surface. At the same time, the hydrolysis reaction of tin tetrachloride pentahydrate leads to the increase of tin oxide hydrate (step II). Then the primary carbon spheres will adsorb the tin oxide hydrate via dehydration of the OH group (a1). It is well known that the viscosity of glycol is 18 times greater than that of water, which makes it difficult for particles to diffuse and participate in the dehydration process rapidly [15]. Therefore, in high viscosity solvent (V_{water}:V_{glycol} = 1:1), the tin oxide hydrate and oligosaccharides will be restricted in a specific area and need more time to diffuse elsewhere. So with the growing of the tin oxide hydrate layer (or carbon layer) the concentration of tin oxide hydrate (or oligosaccharides) will decrease apparently in a period of time until the surrounding tin oxide hydrate disperses homogeneously. Therefore the tin oxide hydrate far away from the as-prepared SnO_2–C composite could not be adsorbed onto the surface continuously. Under this circumstance, the as-prepared high concentration of oligosaccharides particles will react with the SnO_2–C composite, resulting in the second layer of oligosaccharides (a2). After carbonisation of the oligosaccharides, the second carbon shell is formed. Then, with the decreasing of oligosaccharides and increasing of tin oxide hydrate around the SnO_2–C composite, the outer shell starts to react with the high concentration of tin oxide hydrate again, resulting in the second layer of tin oxide hydrate (a3). So the well-defined carbon layer and the tin oxide layer are assembled layer by layer via the chemically induced dehydration with the decreasing and increasing of tin oxide hydrate or oligosaccharides, respectively (a4). The prepared SnO_2–C composite was calcinated, leaving the HS-SnO_2 microspheres (a5).

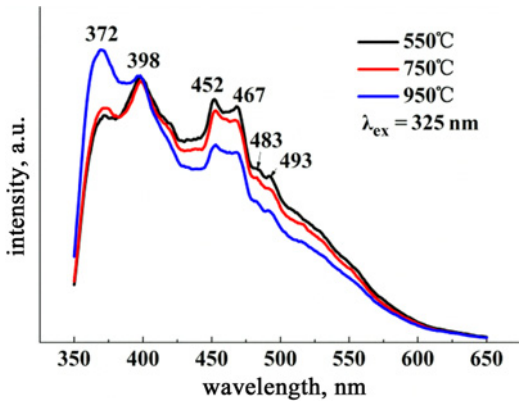

Figure 5 *Room temperature PL spectra of MHS-SnO_2 calcinated at different temperatures*

In addition, in high viscosity solvent, the nucleation and growth process in our experiment will be more homogeneous which will increase the smoothness and the uniformity of the as-prepared MHS-SnO_2.

3.4. Photoluminescence properties: The PL spectra of the obtained MHS-SnO_2 calcinated at different temperatures were investigated and the results are shown in Fig. 5. PL spectra are recorded under exactly the same conditions for all samples.

A strong broad emission band located about 350–600 nm which almost covers the whole visible region is observed. Four strong emmition peaks at 372, 398, 452 and 467 nm can be seen for all samples in Fig. 5. In addition, with the increase of calcinating temperature, the intensity of the peak at 372 nm increases while the intensity of the peaks at 452 and 467 nm decreases. Therefore it is reasonable to deduce that the luminescence mechanism of the peak at 372 nm is different from that of the peaks at 452 and 467 nm. The peak intensity of 452 nm decreases with the increase of grain size, which indicates that the peak is associated with nanocrystal grains or tin interstitials [16] resulting from the size effect of the MHS-SnO_2. The peak at 467 nm is attributed to electron transition mediated by defect levels such as oxygen vacancies in the bandgap that arise from the hydrothermal growth process [17]. The peak at 372 nm is attributed to bandgap emission, which is closely related with the concentration of impurity and defects [18]. It can be observed that the intensity of the peak at 398 nm remains almost same with increasing of the annealing temperature. Therefore it can be deduced that the peak at 398 nm is because of structural defects or luminescence centres that are independent of oxygen vacancies, which is consistent with the related investigation [19]. Hu *et al.* [20] and Tan *et al.* [19] have reported two weak peaks at 483 and 493 nm and ascribed them to other defects which are still not clear.

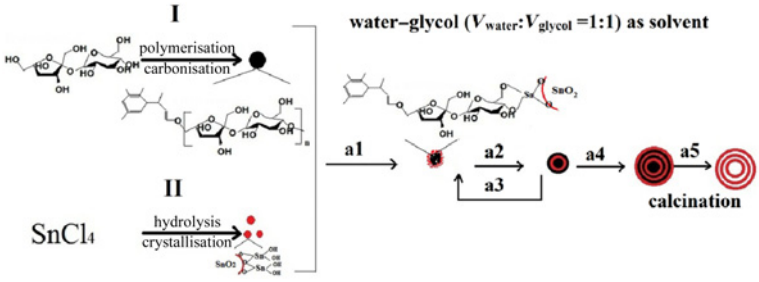

Figure 4 *Schematic illustration of the growth mechanism of MHS-SnO_2*

4. Conclusions: In summary, we have demonstrated a simple route to synthesise MHS-SnO_2 by using the mixture of glycol and water as the solvent. This approach provides a new controllable route to synthesise SnO_2 products with different morphologies. The FESEM results show that the as-prepared product exhibits a multilayered hollow spherical structure with uniform shape. The TEM and HRTEM results illustrate that the multilayered hollow microspheres have a three layered structure and the shell of the hollow microspheres is composed of single crystalline nanoparticles. XRD patterns manifest that the as-prepared product has a perfect rutile crystalline lattice. Based on careful observation and analysis, a self-assembly mechanism relating to the high viscosity of glycol for the formation of the MHS-SnO_2 is proposed. Raman investigation of MHS-SnO_2 shows that the Raman-active peaks become stronger and sharper with increasing calcinating temperature. The lower lattice space symmetry and lattice defects lead to the occurrence of additional non-Raman active peaks. A strong broad emission band located at about 350–600 nm which almost covers the whole visible region has been observed for all three samples and attributed to tin interstitials, oxygen vacancies and structural defects. The intensity of the PL peak at 398 nm remains almost unchanged at different calcinating temperatures and manifests that the peak is independent of oxygen vacancies. Such material with controlled morphologies and large specific surface area may exhibit a special performance in green energy storage, solar cells, optical devices and gas-sensing applications.

5. Acknowledgments: This work was supported by the National Natural Science Foundation of China (grant no. 61373072) and the National Key Scientific Instruments and Equipment Development Special Fund (2011YQ14014506 and 2011YQ14014507), the Oriented Award Foundation for Science and Technological Innovation, Inner Mongolia Autonomous Region, China (2012) and the Fundamental Research Funds for the Central Universities (grant no. FRF-TP-13-021A).

6 References

[1] Yang H.X., Qian J.F., Chen Z.X., *ET AL.*: 'Multilayered nanocrystalline SnO_2 hollow microspheres synthesized by chemically induced self-assembly in the hydrothermal environment', *J. Phy. Chem. C*, 2007, **111**, pp. 14067–14071

[2] Chuah L.S., Yaacob M.Y., Fan M.S., *ET AL.*: 'Synthesis, characterization and optical properties of Ni-doped nanocrystalline SnO_2', *Optoelectron. Adv. Mater-Rapid Commun.*, 2010, **4**, pp. 1542–1545

[3] Iqbal M.Z., Wang F., Feng T., *ET AL.*: 'Facile synthesis of self-assembled SnO nano-square sheets and hydrogen absorption characteristics', *Mater. Res. Bull.*, 2012, **47**, pp. 3902–3907

[4] Nayral C., Ould-Ely T., Maisonnat A., *ET AL.*: 'A novel mechanism for the synthesis of tin/tin oxide nanoparticles of low size dispersion and of nanostructured SnO_2 for the sensitive layers of gas sensors', *Adv. Mater.*, 1999, **11**, pp. 61–63

[5] Fukai Y., Kondo Y., Mori S., *ET AL.*: 'Highly efficient dye-sensitized SnO_2 solar cells having sufficient electron diffusion length', *Electrochem. Commun.*, 2007, **9**, pp. 1439–1443

[6] Wang W.W., Zhu Y.J., Yang L.X.: 'ZnO-SnO_2 hollow spheres and hierarchical nanosheets: hydrothermal preparation, formation mechanism and photocatalytic properties', *Adv. Fun. Mater.*, 2007, **17**, pp. 59–64

[7] Pekarek K.J., Jacob J.S., Mathiowitz E.: 'Double-walled polymer microspheres for controlled drug release', *Nature*, 1994, **367**, pp. 258–260

[8] Xie J., Varadan V.K.: 'Synthesis and characterization of high surface area tin oxide/functionalized carbon nanotubes composite as anode materials', *Mater. Chem. Phy.*, 2005, **91**, pp. 274–280

[9] Wang Y., Su F., Lee J.Y., *ET AL.*: 'Crystalline carbon hollow spheres, crystalline carbon–SnO_2 hollow spheres, and crystalline SnO_2 hollow spheres: synthesis and performance in reversible li-ion storage', *Chem. Mater.*, 2006, **18**, pp. 1347–1353

[10] Lou X.W., Yuan C., Archer L.A.: 'Shell-by-shell synthesis of tin oxide hollow colloids with nanoarchitectured walls: cavity size tuning and functionalization', *Small*, 2007, **3**, pp. 261–265

[11] Sangeetha P., Sasirekha V., Ramakrishnan V.: 'Micro-Raman investigation of tin dioxide nanostructured material based on annealing effect', *J. Raman Spectrosc.*, 2011, **42**, pp. 1634–1639

[12] Zhou J.X., Zhang M.S., Hong J.M.: 'Raman spectroscopic and photoluminescence study of single-crystalline SnO_2 nanowires', *Solid State Commun.*, 2006, **138**, pp. 242–246

[13] Dieguez A., Romano-Rodriguez A., Vila A., Morante J.R.: 'The complete Raman spectrum of nanometric SnO_2 particles', *J. Appl. Phy.*, 2001, **90**, pp. 1550–1557

[14] Titirici M.M., Antonietti M., Thomas A.: 'A generalized synthesis of metal oxide hollow spheres using a hydrothermal approach', *Chem. Mater.*, 2006, **18**, pp. 3808–3812

[15] Tsierkezos N.G., Molinou I.E.: 'Thermodynamic properties of water + ethylene glycol at 283.15, 293.15, 303.15, and 313.15 K', *J. Chem. Eng. Data*, 1998, **43**, pp. 989–993

[16] Jia T., Wang X., Wang W., *ET AL.*: 'Facile synthesis of SnO_2 hollow microspheres and their optical property', *J. Wuhan Univ. Technol.*, 2011, **26**, pp. 302–305

[17] Zhu Z., Ma J., Luan C., *ET AL.*: 'Structure and photoluminescence properties of epitaxial SnO_2 films grown on α-Al_2O_3 (012) by MOCVD', *J. Lumin.*, 2011, **131**, pp. 88–91

[18] Jeong J., Choi S.P., Chang C.I., *ET AL.*: 'Photoluminescence properties of SnO_2 thin films grown by thermal CVD', *Solid State Commun.*, 2003, **127**, pp. 595–597

[19] Tan L., Wang L., Wang Y.: 'Hydrothermal synthesis of SnO_2 nanostructures with different morphologies and their optical properties', *J. Nanomater.*, 2011, **2011**, pp. 1–10

[20] Hu J.Q., Ma X.L., Shang N.G., *ET AL.*: 'Large-scale rapid oxidation synthesis of SnO_2 nanoribbons', *J. Phy. Chem. B*, 2002, **106**, pp. 3823–3826

doi: 10.1049/mnl.2013.0681